RSC Sustainability

PAPER

View Article Online
View Journal | View Issue

Check for updates

Cite this: *RSC Sustainability*, 2025, **3**, 3567

# Collagen from skipjack tuna skin waste enhances cellular proliferative activity, vascularization potential and anti-inflammatory properties of nanofibrous and hydrogel scaffolds†

Tejaswini Petkar, Marie Andrea Laetitia Huët, Devesh Bekah, Itisha Chummun Phul, Nowsheen Goonoo and Archana Bhaw-Luximon *

Marine collagen is gaining prominence in tissue engineering as a sustainable biomaterial and a safe alternative to mammalian collagen. Collagen was extracted from skipjack tuna skin waste using the acetic acid extraction method with a yield of 10.02 ± 2.69%. SDS PAGE indicated the presence of α-tropocollagen chains (α1 and α2) with molecular weights of 120–140 kDa, a β dimer at ~200 kDa, and a γ component trimer at ~250 kDa. The hydroxyproline content of the extracted collagen (14.42 ± 0.11%) was higher than reported values, indicating better structural integrity and thermostability. The extracted collagen was added to three scaffolds namely a polydioxanone/poly(3-hydroxybutyrate-*co*-3-hydroxyvalerate) (PDX/PHBV 50/50, 10 wt%) nanofibrous mat, polysucrose methacrylate hydrogel (PSucMA 5 wt%) and cellulose-lignin (Cel-lig 2 wt%) hydrogel. *In vitro* experiments were performed using RAW 264.7 macrophages to assess inflammatory activity, human dermal fibroblasts (HDFs) to assess proliferative activity and Human Umbilical Vein Endothelial Cells (HUVECs) to assess the vascularization potential of the scaffolds with collagen. The macrophages showed a reduced inflammatory M1 phenotype in the presence of collagen, while HUVECs and HDFs showed enhanced proliferation. Overall, fish skin waste collagen has the potential to enhance the performance and allows the engineering of multitasking scaffolds.

Received 19th May 2025
Accepted 29th June 2025

DOI: 10.1039/d5su00352k

rsc.li/rscsus



### Sustainability spotlight

Waste valorisation and sustainable resource utilisation support the blue circular economy. Extracting collagen from skipjack tuna skin waste offers an innovative waste management solution for small islands like Mauritius by converting marine remnants into valuable biomaterials. Our study employs a cost-effective, environmentally friendly acetic acid extraction method with industrial scalability, yielding collagen with intact α-, β-, and γ-chains and high hydroxyproline content. This marine collagen, incorporated into hydrogels and nanofiber scaffolds, promotes cell proliferation and angiogenesis and reduces inflammation, making it ideal for tissue regeneration applications. This work highlights sustainable resource usage to lower the environmental footprint and advance the global bioeconomy. It is in line with the United Nations Sustainable Development Goals 3 and 14.

## 1 Introduction

The extracellular matrix (ECM) plays an active role in cell proliferation, differentiation and migration. There exists a synergy between the ECM and cells; the ECM provides a support structure and the cells in return repair and maintain the ECM through the production of proteins, glycoproteins, sugars and glycosaminoglycans.[1] Proteins are a major component of the ECM and can be grouped into structural or fibrous proteins (collagen and elastin) and non-structural proteins or glycoproteins (fibronectin). Collagen is an important constituent of this ECM, where it exists as fibrils of collagen types I, II, III, V and XI, with type I being the most abundant. It provides tensile strength and thus supports cell processes such as adhesion and migration. Fibroblasts play an important role in tissue regeneration after a wound and are the main cells that produce and maintain collagen. This collagen is in the form of procollagen, which is cleaved by proteases for assembly in the ECM. The use of collagen in tissue engineering scaffolds has been guided by the presence of collagen in the ECM and its role in cell sensing and migration.[2–4] In the wound environment, collagen is important for platelet aggregation, inflammation modulation, angiogenesis, granulation tissue formation and re-epithelialization in an integrin signalling-dependent manner.[5,6]

*Biomaterials, Drug Delivery and Nanotechnology Unit, Centre for Biomedical and Biomaterials Research, University of Mauritius, Réduit 80837, Mauritius. E-mail: a.luximon@uom.ac.mu; Tel: (+230) 464 3781*

† Electronic supplementary information (ESI) available. See DOI: https://doi.org/10.1039/d5su00352k

Collagen has been shown to regulate inflammation.[7–9] During inflammation, soluble collagen fragments attract immune cells like macrophages to the wound site to clear microbes and necrotic tissues. This allows the wound site to move from the pro-inflammatory to the anti-inflammatory stage, thus leading to the proliferative phase of wound healing. Angiogenesis and keratinocyte migration are triggered by collagen's influence on signalling pathways.[10–12]

Bovine collagen type I has long been used in biomedical applications to treat tissue injuries.[13–17] However, severe infections (zoonoses), including bovine spongiform encephalopathy, avian and swine influenza, and foot-and-mouth disease in bovines, pigs, and buffaloes are persistent problems for scaffold manufacturing. The use of porcine- and bovine-derived products is also forbidden by religious constraints.

Fish collagen is explored as a replacement for bovine collagen.[18,19] Fish and bovine collagen do not have the same characteristics; for instance, the $M_w$ of the original native bovine collagen is several times higher than that of fish collagen.[20] Collagen exists in its triple helix form and enzymatic action is required to degrade it for use in tissue engineering scaffolds and other applications. Fish collagen is often considered a more sustainable option, reducing waste in the fishing industry. Bovine collagen may have a higher environmental impact due to factors such as land use and methane emissions associated with cattle farming.

Collagen extract derived from Nile tilapia skin was tested on full-thickness wounds on the backs of rats.[21] The tilapia collagen extract was applied topically on the wound area. The improved wound healing observed was attributed to enhanced recruitment and activation of macrophages producing chemotactic growth factors, fibroblast proliferation, and angiogenesis, upon the upregulation of transforming growth factor beta 1 (TGF-β1), basic fibroblast growth factor (bFGF), and alpha-smooth muscle actin (α-SMA) gene expression and enhanced TGF-β1 and vascular endothelial growth factor (VEGF) expression.

Commercial collagen mainly from bovine sources has been tested mostly in the form of hydrogels combined with other materials to enhance mechanical properties. For instance, a collagen hydrogel bioconjugate through cross-linking with chitosan loaded with *N*-acetylcysteine and ε-poly-lysine was evaluated in a model of excisional wounds in mice. The results showed improvement in tissue healing, with reduced lesion size and reduced inflammation.[22]

Fish collagen from the scales of *Cyprinus carpio* was cross-linked with 1-ethyl-3-(3-dimethylaminopropyl) carbodiimide (EDC) and *N*-hydroxysuccinimide (NHS), and its antimicrobial activity was determined using *S. aureus* bacteria and cytotoxicity on mouse fibroblast cells (NIH/3T3) by MTT assay.[23] No zone of inhibition was observed around the EDC/NHS-crosslinked chitosan and the MTT assay did not show cytotoxicity after 72 hours.

A recent study demonstrated the use of tuna derived collagen in scaffolds as an optimal microenvironment for the *in vitro* release of phycocyanin as a bioactive molecule. The findings demonstrated that adding increasing amounts of bluefin tuna derived collagen to chitosan hydrogels led to a highly interconnected porous structure, improved swelling rate, enhanced elasticity and reduced degradation across varying pHs, with significant changes seen upon addition of 50% collagen. At this protein concentration, a faster phycocyanin release was also observed in acidic medium (pH 5.5 *vs.* pH 7.4), implicating its potential as a controlled drug-release system. The addition of collagen to the scaffold also enhanced hydrophilicity, which is important in tissue regeneration. The water-rich structure of the composite hydrogel mimics the hydrated microenvironment of the ECM in the human body, facilitating the transport of oxygenated nutrients within the gel pores and preventing tissue dehydration and/or necrosis, while supporting cellular adherence and proliferation, thus creating an optimal hydrated environment for cellular growth and proliferation.[24]

Approximately 70% of fish are processed before being sold, resulting in enormous amounts of solid waste from processes such as beheading, separating fins and scales, and filleting with 40% of fish mass being wasted. The huge volume of fish waste poses challenges for urban planning. Fish skin has found uses as fish leather and as a valuable source of ingredients in animal food as well as cosmeceuticals and nutraceuticals for human consumption. This study aims to demonstrate that collagen derived from tuna fish skin waste can promote cell proliferation and migration in both nanofibrous and hydrogel scaffolds and influence the inflammation phase towards tissue regeneration (Scheme 1).

Three scaffolds were used, and collagen was added to a polydioxanone/poly(3-hydroxybutyrate-*co*-3-hydroxyvalerate) (PDX/PHBV 50/50, 10 wt%) nanofibrous mat, polysucrose methacrylate hydrogel (PSucMA 5 wt%) and cellulose-lignin (Cel-lig 2 wt%) hydrogel. These scaffolds were chosen for their *in vitro* and *in vivo* biocompatibility as previously demonstrated by us.[25–27]

An electrospun mat consisting of blended PDX/PHBV nanofibers was chosen for its established properties in the biomedical field, particularly in tissue regeneration and wound healing. Electrospun mats are especially favored for their intrinsic ability to imitate the natural ECM structure. PDX provided similar mechanical properties to collagen and influenced cellular migration and adhesion, while PHBV, a piezoelectric material, promoted fibroblast proliferation.[25,28–30] Together, they could influence essential events involved in wound healing.

The polysucrose MA hydrogel was chosen for its established potential in wound healing.[26,31,32] The scaffold was highly porous, reproducible and controllable. Its biocompatibility was demonstrated *in vitro* and *in vivo*. It has also shown favorable tissue regeneration and scarless controlled wound closure, outperforming commercially available gels. The methacrylation of sucrose, a natural polysaccharide, influenced the permeability of the scaffold, enabling controlled molecule loading and release.

The cellulose-lignin hydrogel was chosen for its suitability as a well-developed three-dimensional hydrogel network with enhanced antibacterial properties.[27] Cellulose and lignin are both value-added, natural and non-toxic polymers, derived from

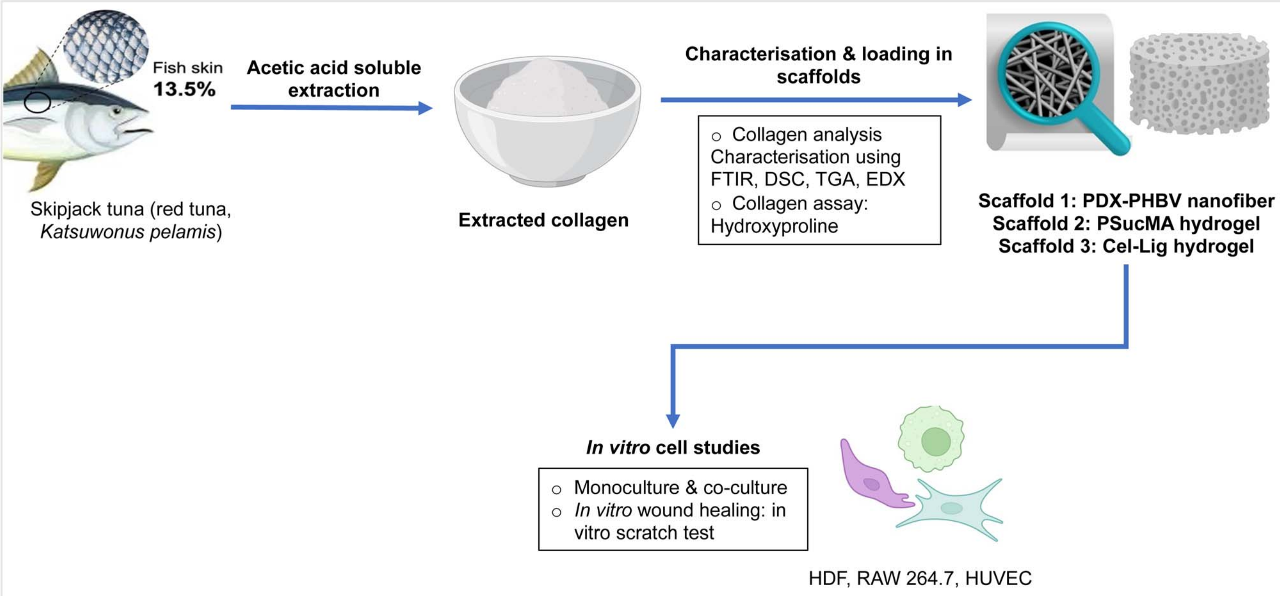


Scheme 1 Fish skin derived collagen to promote tissue regeneration. Designed using http://Biorender.com.

agricultural wastes. Cellulose is abundant, hydrophilic, biocompatible and easily biodegradable and thus inherently exhibits several desirable characteristics for tissue engineering and wound healing. Lignin's properties further enhance the hydrogel's functionality through its innate antibacterial, anti-UV and antioxidant properties. This makes the scaffold highly desirable for biomedical applications including tissue engineering and antimicrobial coatings.[27,33–35]

## 2 Experimental

### 2.1 Materials

Sodium hydroxide pellets (AR grade) were purchased from Central Drug House (P) Ltd, India. 1-Butanol (99.9%) was purchased from Sigma-Aldrich, USA. Glacial acetic acid (99.7%) and sodium chloride (AR ACS grade; 99.5% purity) were purchased from Loba Chemie Pvt. Ltd, India. Anhydrous disodium hydrogen phosphate (98% purity) was purchased from SD Fine Chem Ltd, India. The soluble form of marine collagen (type I) was purchased from Vecteur Sante, Aubergenville, France and used as a control. Chloramine T trihydrate (ACS grade; 98% purity) and sodium acetate trihydrate (analytical grade; 99–101% purity) were purchased from Sigma Aldrich, Germany. Citric acid monohydrate powder (≥99.0% purity; ACS reagent) and 2-propanol (≥99.8% purity; ACS and GC grades) were purchased from Sigma Aldrich, St. Louis, USA. Glacial acetic acid (99.7%) was purchased from Loba Chemie Pvt. Ltd, India. *p*-Dimethyl amino benzaldehyde (≥99.8% purity; ACS grade) was purchased from Sigma Aldrich, India. Sodium hydroxide pellets (AR grade) and hydrochloric acid (1.18; AR grade) were purchased from Central Drug House (P) Ltd, India. Hydroxyproline standard (RM052) was purchased from Himedia, USA. Polydioxanone or PDX (Resomer X 206S; inherent viscosity: 2.0 and $M_W = 1.01 \times 105$ g mol$^{-1}$) was purchased from Evonik, Germany. Poly(3-hydroxybutyrate-*co*-3-hydroxyvalerate) or PHBV (HV content: 12 mol% and molar mass: 400–600 kDa) was bought from Sigma-Aldrich. 1,1,1,3,3,3-hexafluoroisopropanol (HFIP) purchased from Apollo Scientific (UK) was used as received. Hydroxyapatite (HA) with an approximate particle size of 100 nm and 98.5% purity was bought from American Elements (USA). Polysucrose (Ficoll®400) with an average molecular weight (Mw) of 400 000 supplied by Serva Electrophoresis was used as received. Epichlorohydrin was bought from Sigma-Aldrich, Germany. Dimethylformamide (DMF), lithium chloride (LiCl), triethylamine (TEA) and ammonium persulfate (APS) were purchased from Sigma Aldrich. Methacrylic anhydride, ethylene glycol dimethacrylate (EGDMA) and tetramethylethylenediamine (TEMED) were obtained from Aldrich Chemical Co.

Human Dermal Fibroblasts (HDFs), RAW 264.7 macrophages and Human Umbilical Vein Endothelial Cells (ECACC certified) and their respective media: fibroblast growth medium, endothelial cell growth medium, RPMI, and fetal bovine serum (FBS), along with penicillin/streptomycin antibiotics and Dulbecco's Phosphate Buffered Saline were purchased from Sigma Aldrich. Propidium iodide and fluorescein diacetate were purchased from Thermo Fisher Scientific, USA. CellTracker™ Green 5-chloromethylfluorescein diacetate (CMFDA) and CellTracker™ Red CMTPX were purchased from Invitrogen, Thermo Scientific, Oregon, USA.

### 2.2 Acetic acid extraction of collagen from fish skin

**2.2.1 Collection and storage of fish skin.** Collagen was extracted from the skin of skipjack tuna (*Katsuwonus pelamis*) locally known as red tuna. The fresh skin was collected from Hassen Taher Seafoods Ltd, Mauritius. The skin was washed under cold tap water. The flesh and scales were scraped and removed. The skin was washed again in cold distilled water. This clean skin was stored at −20° until further use.

**2.2.2 Extraction procedure.** The frozen skin was thawed in cold distilled water. 100 g skin was washed in physiological saline (PBS) and cold distilled water. The skin was pre-treated with 0.1 M NaOH (1 : 10 w/v) at 4 °C for 48 h with a change of solution every 2 h until the solution turned least turbid. The pieces were then washed and treated with 10% butanol (1 : 10 w/v) for 24 hours at 4 °C.

The skin was homogenized with 0.5 M acetic acid (w/v) (1 : 15) using an Ika T-25 digital ULTRA-TURRAX® model homogenizer at 20 000 rpm. The homogenate was precipitated using 5% w/v sodium chloride and left overnight at 4 °C for the acid soluble collagen to settle. The solution was centrifuged for at 3100 G 25 minutes at 3 °C using a Thermo Fisher Scientific SL 16 R model, and the collected precipitate was redissolved in 0.5 M acetic acid to ensure complete solubilization. The precipitation process using 5% w/v sodium chloride was repeated to ensure maximum protein extraction. The precipitate was eventually solubilized in 0.1 M acetic acid and dialyzed using SERVAPOR dialysis tubing (MWCO: 12 000–14 000 Da) in three steps for three days: 20 mM disodium hydrogen phosphate ($Na_2HPO_4$) for 1 h followed by 0.05 M acetic acid (changed twice at regular intervals) and finally distilled water for a day and a half (changed thrice per day). The entire extraction process was performed under cold conditions.

The volume of the acid soluble form of collagen for each extraction was noted, its yield was determined using eqn (1), and an aliquot of the extracted protein was lyophilized to form a sponge form of collagen. All samples were stored at 4 °C until further analysis.

$$\text{Yield }(\%) = \frac{(\text{Mass of dry collagen})}{(\text{Mass of wet skin})} \times 100 \qquad (1)$$

**2.2.3. SDS-PAGE.** SDS-PAGE was conducted using an omniPAGE Mini apparatus (Cleaver Scientific Ltd). Extracted collagen replicates were dissolved in 0.05 M acetic acid to form 7.5 mg $ml^{-1}$ solutions. The samples were suspended in lysis buffer (1 : 1) containing 4 mL glycerol, 2 mL β-mercaptoethanol, 1.2 g SDS, 5 ml stacking buffer (pH 6.8) and 0.03 g bromophenol blue and dissolved by heating at 93 °C for 5 minutes, followed by centrifugation at 8500×G at 4 °C for 7 minutes. 15 µL of each extracted collagen replicate (lanes I to III) was loaded onto wells of an 8% gel and subjected to electrophoresis. After the run, the gel was fixed with a solution containing ethanol, acetic acid and distilled water (5 : 1 : 4) for 30 minutes. The gel was washed with a solution containing methanol, acetic acid and distilled water (5 : 1 : 4) for 5 minutes and stained with Coomassie Brilliant Blue solution for 45 minutes. This was followed by washing with ultrapure water and the gel washing solution alternately for 5 minutes each. Bands were viewed under blue light.

## 2.3 Fabrication of scaffolds with or without collagen

**2.3.1 Electrospun PDX/PHBV nanofiber.** PDX/PHBV 50/50 solutions were prepared in HFIP at a concentration of 100 mg $ml^{-1}$ and stirred at 300 rpm for 24 hours. Electrospinning was carried out using a bottom-up NE300 laboratory scale nanospinner (Inovenso) at a voltage of +23 kV, a flow rate of 1 ml $h^{-1}$ and a tip to collector distance of 140 mm. Continuous fibres were collected as non-woven fibre mats on a static grounded aluminium target. Similar parameters were used for the production of PDX/PHBV/collagen fibres, where 10 wt% collagen was added with respect to the total polymer content.

**2.3.2 Synthesis of hydrogels**

*2.3.2.1 Polysucrose-methacrylate (PSucMA) hydrogels.* PSucMA hydrogels have been synthesized using established protocols.[26,36] Briefly, to prepare methacrylated polysucrose, 5 g of PSuc (Mw 400 000) was solubilized in 25 ml of 10 wt% dimethylformamide/lithium chloride at 90 °C under vacuum. Triethylamine (TEA) and methacrylic anhydride (MA) were added to the solution at 60 °C and allowed to stir under vacuum for 16 hours. The volume of methacrylic anhydride (6588 µl) amounted to 0.5 molarity of the hydroxyl group in 5 g of PSuc and the volume of TEA (310 µl) determined accordingly (mol ratio TEA : MA = 0.05). PSucMA was then precipitated using acetone, dried under vacuum and solubilized in distilled water. The solution was dialyzed for a week and freeze-dried.

PSucMA (5 wt%) was then solubilized in distilled water and crosslinked using ethylene glycol dimethacrylate (EGDMA) in the presence of tetramethylethylenediamine (TEMED) and ammonium persulfate (APS). The volume of EGDMA amounted to 3 molarity of the methacrylate groups determined by $^1$H NMR. 10 wt% collagen with respect to the amount of PSucMA was loaded *in situ* during the synthesis of PSucMA hydrogels. 125 mg of PSucMA and 12.5 mg of collagen were solubilized in 2.5 ml aqueous solution. The solution was then crosslinked using EGDMA in the presence of 50 µl TEMED and 50 µl APS. The hydrogels were washed thrice in distilled water.

*2.3.2.2 Cellulose-lignin (Cel-Lig) hydrogels.* Cellulose-lignin hydrogels were synthesized as reported by Huët *et al.*[27] Briefly, sugarcane bagasse (SCB) cellulose was suspended in a premixed solution of sodium hydroxide (6 wt%) and urea (4 wt%) at a concentration of 1.4 wt%. The suspension was stirred at room temperature for 10 minutes and frozen at −20 °C overnight. The latter was then thawed and stirred at maximum speed at room temperature. A total of 0.6 wt% of extracted SCB lignin was added to the cellulose solution, followed by the addition of 10 wt% collagen. The resulting solution was stirred for 30 minutes. (±)-Epichlorohydrin was then added drop by drop (10%) to the cellulose–lignin–collagen solution. The latter was stirred at 25 °C for 1 hour, cast in wells and kept at 50 °C overnight in a water bath. The hydrogels were then washed with distilled water and then freeze-dried.

## 2.4 Characterization techniques

The chemical, elemental and thermal properties of extracted collagen were determined using Fourier Transform Infrared Spectroscopy (FTIR), Energy Dispersive X-ray (EDX), Differential Scanning Calorimetry (DSC) and Thermogravimetric Analysis (TGA). The hydroxyproline content of collagen was also assessed. The porosity and water affinity of the scaffolds were determined using scanning electron microscopy (SEM), contact angle measuring and equilibrium swelling studies.

**2.4.1 Infrared spectroscopy (FTIR).** The composition of collagen was studied using an ALPHA FTIR spectrometer (BRUKER) against air as the background in the range of 400–4000 $cm^{-1}$.

**2.4.2 Energy dispersive X-ray (EDX) spectroscopy.** Dry collagen samples were mounted on aluminium stubs *via* a piece of carbon tape and subjected to elemental analysis using an energy dispersive X-ray spectroscopy (EDX) (Bruker X-Flash 6160) mounted on a Tescan Vega 3 scanning electron microscope. All of the analyses were performed at a voltage of 20 kV, using a 30 s scan duration.

**2.4.3 Thermal analyses.** The thermal properties of collagen were determined through Differential Scanning Calorimetry (DSC) and Thermogravimetric Analysis (TGA). DSC was conducted using a DSC 200 F3 Maia® thermal analyzer (NETCZH, India). Collagen samples were weighed in an aluminium crucible heated from 20 to 350 °C at a rate of 10 K $min^{-1}$. For TGA analysis of collagen, a TG 209 F3 Tarsus® thermal analyzer (NETCZH, India) was used. Collagen samples were weighed and heated to 1000 °C at a rate of 10 K $min^{-1}$.

**2.4.4 Hydroxyproline analysis of collagen.** To perform the analysis, the following reagents were prepared: hydroxyproline standard: a standard of 100 μg $mL^{-1}$ hydroxyproline standard solution was prepared using 0.01 N HCl as the stock solution. Fresh Chloramine T reagent (0.056 M): 1.27 g was dissolved in 20 mL of 50% 2-propanol and brought to 100 mL using citric acid buffer. Fresh *p*-dimethyl amino benzaldehyde (pDAB) reagent (3.33%): 1.625 g of *p*-dimethyl amino benzaldehyde powder was dissolved in 16.25 mL of 50% 2-propanol, 16.25 mL of 0.01 M HCl, and 16.25 mL of 3.15 M HCl. Citrate buffer (pH 6)-100 mL: 5 g citric acid monohydrate, 12 g sodium acetate trihydrate and 3.4 g sodium hydroxide were dissolved in 1.2 mL glacial acetic acid and made up to 100 mL using distilled water.

A hydroxyproline standard (100 μg $mL^{-1}$) was prepared using 0.01 N HCl as the stock solution. From this, dilutions (0–2.5 μg) were prepared in triplicate. To each dilution, 1 mL freshly prepared chloramine T trihydrate reagent was added and incubated for 20 minutes, followed by 3.15 M HCl[37] for 5 minutes, and finally freshly prepared *p*-dimethyl amino benzaldehyde (pDAB) (3.33%). After adding pDAB, the solutions were placed in a water bath at 60 °C for 20 minutes. Their absorbance was measured at 557 nm.

A total of 200 mg $mL^{-1}$ collagen samples (w/v) were digested in 6 N HCl at 106–110 °C for 8–16 h. To each 2 mL of sample hydrolysate, 1 mL of chloramine T reagent was added and incubated for 20 minutes, followed by 3.15 M HCl for 5 minutes, and finally *p*-dimethyl amino benzaldehyde (pDAB) (3.33%). After adding pDAB, the sample was placed in a water bath at 60 °C for 20 minutes. This was done in triplicate for all samples, and their absorbance was measured at 557 nm.

**2.4.5 SEM.** The collagen loaded scaffolds were mounted on aluminium stubs and sputter-coated with gold/palladium for 120 s. They were then imaged using a TESCAN VEGA 3 LMU field emission scanning electron microscope (SEM) at 20 kV at a working distance of 5–10 mm.

The average pore size of the scaffolds and the average fibre diameters of the electrospun mats were determined from SEM images as reported previously.

SEM imaging was also used to assess the surface roughness of the cellulose-lignin hydrogels by calculating their respective average roughness ($R_a$ value) using the SurfCharJ q1 plugin in Fiji/ImageJ software (USA).

**2.4.6 Equilibrium swelling studies.** The equilibrium swelling studies of all hydrogels were carried out in phosphate buffer solution (PBS) at 37 °C for 38 hours. The dry mass of the hydrogels, $m_d$, was initially measured and the swollen hydrogels were periodically weighed until equilibrium. The percentage swelling was then calculated using eqn (2).

$$\%\ \text{swelling},\ S_t = \left(\frac{m_t - m_d}{m_d}\right) \times 100 \quad (2)$$

where $m_d$ and $m_t$ are the dry mass and swollen mass of the hydrogels at time $t$, respectively.

The contact angles of the electrospun mats were measured using distilled water as a probe liquid with a Kruss Drop Shape Analyzer DSA 25 (Advanced Lab GmbH, Germany).

### 2.5 *In vitro* cell culture studies

Human Dermal fibroblasts (HDFs), RAW 264.7 macrophages and Human Umbilical Vein Endothelial Cells (ECACC certified) were cultured in their respective media: HDFs in fibroblast growth medium, HUVECs in endothelial cell growth medium and RAW 264.7 in RPMI. RPMI was supplemented with 10% foetal bovine serum (FBS) and 1% penicillin/streptomycin.

**2.5.1 Monoculture of HDFs and RAW 264.7 on scaffolds.** The scaffolds were placed in 96-well plates, UV sterilized and disinfected with 70% ethanol immersion for 30 min, followed by 3 consecutive washes in Dulbecco's phosphate buffer solution (DPBS). The hydrogels were incubated in culture media overnight prior to cell seeding.

$2 \times 10^4$ cells (HDFs and RAW) per well were seeded on each scaffold. The culture plates were then incubated under standard conditions (37 °C and 5% $CO_2$) for 14 days respectively and fresh medium was replenished every 3 days. The cell-seeded scaffolds were fixed for SEM using our previously described protocol.[26]

**2.5.2 Co-culture of HDFs and HUVECs on scaffolds.** The scaffolds were placed in 96-well plates, UV sterilised and disinfected with 70% ethanol immersion for 30 min, followed by 3 consecutive washes in Dulbecco's phosphate buffer solution (DPBS). The hydrogels were incubated in culture media overnight prior to cell seeding.

HDFs and HUVECs grown on T75 culture flasks were incubated in 4 ml of 20 μM fluorescent CellTracker™ green 5-chloromethylfluorescein diacetate (CMFDA) and CellTracker™ red CMTPX (Invitrogen, Thermo Fisher, Oregon), respectively, for 1 hour prior to seeding of both cells on each scaffold at a cell density of $1 \times 10^4$ cells per cell type. The cell-seeded scaffolds were imaged using an EVOS fluorescence microscope.

**2.5.3 *In vitro* scratch assay: HDF co-cultured with RAW 264.7 and HUVECs, respectively.** HDFs, HUVECs and RAW 264.7 cells grown in T75 culture flasks were incubated in 4 ml of 20 μM fluorescent CellTracker™ probes for 1 h. HDFs were tagged with CellTracker™ green 5-chloromethylfluorescein diacetate (CMFDA). RAW 264.7 and HUVECs were tagged with CellTracker™ red CMTPX. HDF_RAW264.7 and HDF_HUVEC were co-cultured in 96-well plates at a cell density of $1 \times 10^4$ cells per cell type in each well. After 24 h of culture, the cell layer in each well was scratched using a micropipette tip. The scratch was visualized using the EVOS fluorescence microscope. The sterilized scaffolds were carefully placed in each well ensuring that the scaffold rested at the bottom of the well in contact with the TCPS surface. The cells were allowed to proliferate, and fluorescence images of the cells were taken on day 3. The number of each cell per mm$^2$ in the scratch region was counted using Image J.

### 2.6 Statistical analysis

The data are presented as arithmetic mean ± standard error of mean. Statistical analyses were done with the one-way or two-way analysis of variance (ANOVA) test (OriginPro 8.5, OriginLab Corporation, USA) and *t*-test (GraphPad Prism version 10, USA). A value of $p < 0.05$ was considered statistically significant.

## 3 Results and discussion

### 3.1 Acetic acid soluble extraction and characterization of collagen from tuna fish skin

Fresh skipjack tuna fish (Indian Ocean) skin was collected from local fish shops and frozen at −20 °C until the extraction process.

**3.1.1 Extraction process.** The acetic acid soluble extraction method was chosen over other extraction methods such as pepsin-enzyme digestion, due to its cost-effectiveness and higher potential for industrial scalability. While this extraction method might give rise to a relatively lower yield, it is best suited for this skin source due to its low dermal fibre intertwinement[38] and retains the native structural properties of the extracted collagen.[39,40] The steps in fish collagen extraction did not involve the use of harsh chemicals such as HCl for protein solubilization, ethanol for protein precipitation, and intensive processing to harvest the protein[41] (Scheme 2).

Tuna skin is highly pigmented and fatty, and its treatment with sodium hydroxide and butanol eliminated impurities, thus increasing the purity of the final collagen product. Fish skin solubilization in acetic acid is followed by precipitation with sodium chloride isolating acid-soluble collagen. This process was repeated to increase the protein yield. Acetic acid extraction was also found to contribute to skin depigmentation.[42] The dialysis step enhanced product purity and lyophilization of the product was performed to ensure the stability of collagen for long-term storage.

The freeze-dried collagen was spongy and brown in colour. The yield of collagen was 10.02 ± 2.69% and was found to be generally higher than reported values from other skipjack tuna waste from the Indian and Pacific Oceans[43,44] (Table 1).

Collagen yield differs based on the fish skin thickness, pigmentation and elastic properties.[45] Tuna fish skin is, in general, moderately fatty and highly pigmented resulting in a lower collagen yield compared to other fish sources. It was further observed that despite thorough washing and pretreatment steps, pigment residues had not been completely eliminated throughout the preliminary treatment with sodium hydroxide and butanol.

**3.1.2 SDS PAGE.** The extracted collagen was analysed by SDS PAGE, which showed the presence of three bands assigned to α-tropocollagen chains (α1 and α2) with molecular weights of 120–140 kDa, a β component dimer made of two alpha chains of ∼200 kDa, and a γ component trimer of ∼250 kDa (Fig. S1, ESI†).

**3.1.3 Characterization.** The extracted collagen was characterized and compared with a commercial soluble marine collagen. The commercial collagen was hydrolysed type I collagen, marketed by Vecteur Santé (France), and was available as a soluble powder derived from marine fish.

**3.1.4 FTIR spectroscopy.** The FTIR spectra of the extracted collagen showed the presence of amide bands A, B, I, II, and III (Fig. 1 and Table S1, ESI†) of the peptide bonds in the protein.

Table 1 Overview of collagen yield extracted from skipjack tuna

| Fish anatomy | Collagen yield (%) |
|---|---|
| Skin | 10.02 ± 2.69 |
| Tail tendon (Indian Ocean)[43] | 8.67 ± 0.35 |
| Spine (Pacific Ocean)[44] | 2.47 ± 0.39 |
| Skull (Pacific Ocean)[44] | 3.57 ± 0.40 |

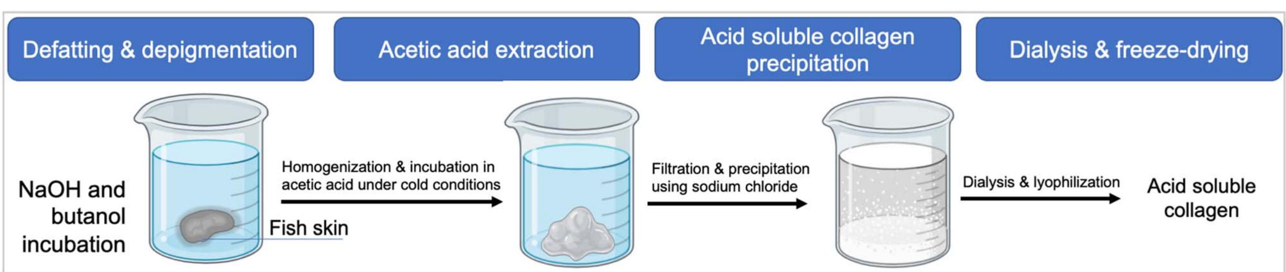


Scheme 2 Collagen acetic acid soluble extraction process. Designed using http://Biorender.com.

 

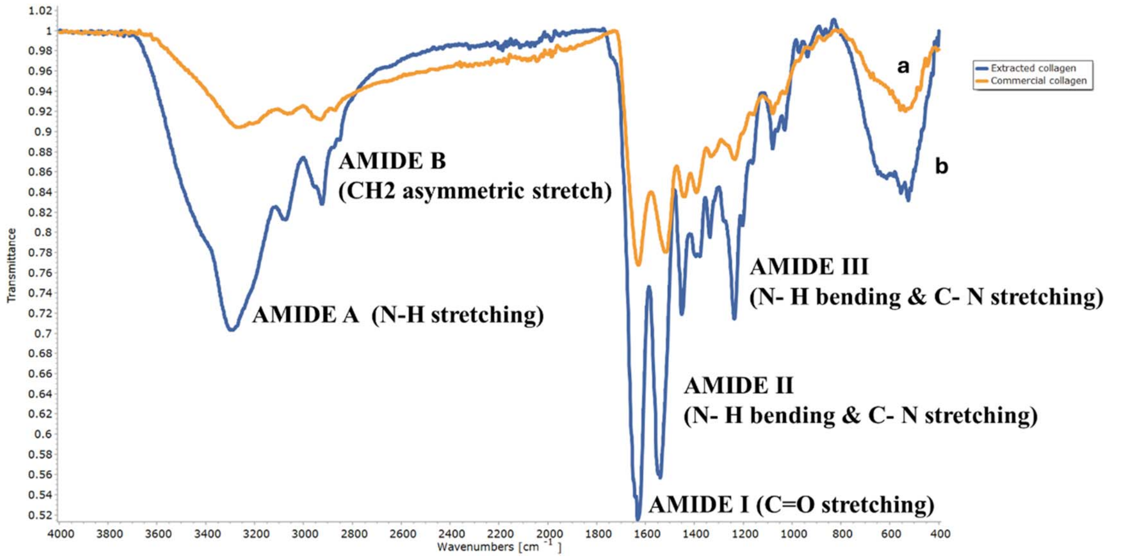


Fig. 1 FTIR spectra of (a) commercial marine collagen and (b) extracted collagen from skipjack tuna fish skin.

The wavelength of amide A (3270 $cm^{-1}$ for commercial collagen and 3292 $cm^{-1}$ for extracted collagen) suggested the NH group was actively involved in hydrogen bonding between the peptide chains, maintaining the triple helical structure, and/or with water indicating a hydrated state[46] **https://www.scielo.br/j/bjmbr/a/VmMPLcmmYL4VRGSzCp57Nqw/**. Both collagen samples displayed the same wavelength for amide I (1628 $cm^{-1}$), denoting similar peptide backbone C=O stretching (70–85%). Amide I is further considered as the fingerprint of a protein's secondary structure composition linked to the polypeptide backbone.[47,48] Amide II (1522 $cm^{-1}$ for commercial collagen and 1545 $cm^{-1}$ for extracted collagen) and amide III (1240 $cm^{-1}$ for commercial collagen and 1237 $cm^{-1}$ for extracted collagen) together indicated N–H bending and C–N stretching, impacting the protein's helical structure. Bands observed around 1080 $cm^{-1}$ and 1030 $cm^{-1}$ in both collagen samples denote CO and CC stretching vibrations and COH and CCO bending vibrations, respectively, revealing the presence of glycation and carbohydrate moieties in collagen, representative of collagen ageing.[49–51]

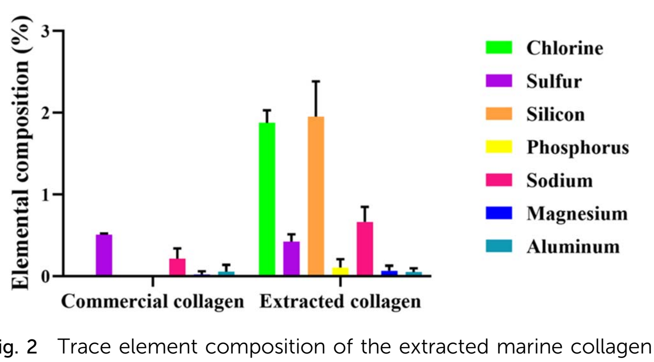


Fig. 2 Trace element composition of the extracted marine collagen compared with commercial marine collagen. Values represent an average of 4 replicates and error bars represent the standard deviation.

**3.1.5 EDX analysis.** EDX analysis was performed to determine the elemental composition of the extracted collagen and commercial collagen (Fig. 2). As expected, carbon (64.9 ± 0.07% for extracted collagen and 66.5 ± 0.27% for commercial collagen) and oxygen (30.0 ± 0.25% for extracted collagen and 32.6 ± 0.23% for commercial collagen) dominated the elemental composition of the collagen samples.

There were some marked differences in the trace element contents between the two collagen samples. Silicon (1.95 ± 0.433% in extracted collagen) is vital for enhancing skin elasticity and strength, for the optimal synthesis of collagen and activation of hydroxylating enzymes.[52] The presence of chlorine (1.877 ± 0.154%) in extracted collagen was probably due to the residual sodium chloride used during the extraction process, persisting despite dialysis.

Sodium (0.210 ± 0.130% for commercial collagen and 0.663 ± 0.185% for extracted collagen) and magnesium (0.023 ± 0.390% for commercial collagen and 0.068 ± 0.061% for extracted collagen) can substitute calcium ions in hydroxyapatite promoting cell adhesion and playing a role in wound healing by triggering cellular migration of fibroblasts and keratinocytes.[53,54]

**3.1.6 Thermal properties of extracted collagen.** The thermal properties of both extracted and commercial collagen were analysed by differential scanning calorimetry (DSC) and thermogravimetric analysis (TGA) to understand the thermosensitive protein's integrity (Fig. 3).

A higher degradation temperature (104.9 °C) was seen for extracted collagen (commercial collagen 91.5 °C). The relatively higher enthalpy of denaturation ($\Delta H$) value was attributed to hydration networks consisting of bound and unbound water molecules around the collagen that were released and evaporated.[55] A second major peak associated with collagen denaturation with the separation of the triple helix and destabilization of the tropocollagen was observed. The extracted collagen showed relatively good thermal resistance (210.3 °C) but lower comparable thermal rigidity and mechanical strength than commercial collagen (234.7 °C), suggesting a less ordered internal structures with fewer crosslinks.[56] The extracted collagen (307.5 °C) degraded at a higher temperature than commercial collagen (277.8 °C), possibly due to higher residual hydroxyproline content in skipjack fish skin.[41,57,58] Overall, the presence of distinct denaturation peaks of both collagen samples in the DSC thermogram demonstrated good protein thermostability. The observed $T_d$ values of fish collagen are generally lower than those of mammalian collagen attributed to inherent lower hydroxyproline levels.[41,59,60]

The protein thermal stability of the extracted collagen due to cross-linking was investigated using thermogravimetric analysis (TGA). The measured mass loss reflected a combination of evaporation and degradation processes.

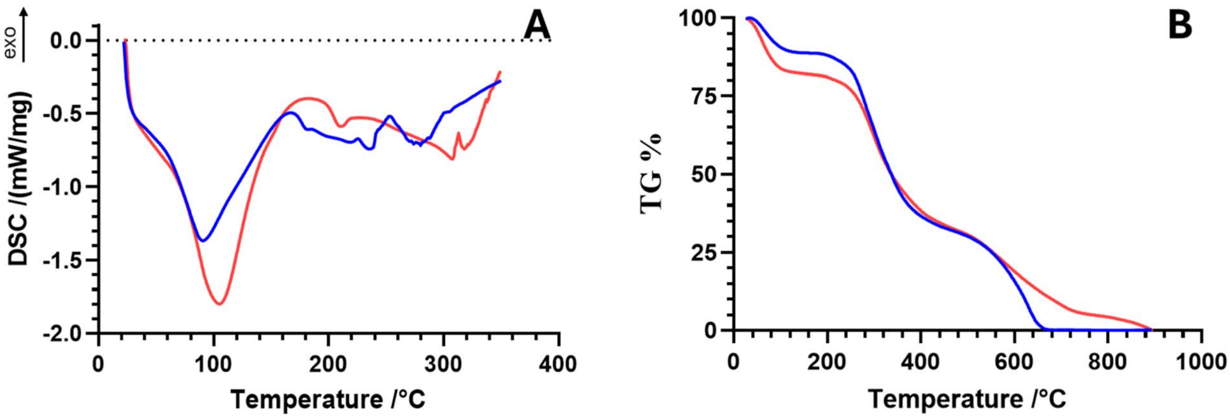


Fig. 3 (A) DSC thermograms of extracted collagen (red) and commercial collagen (blue); (B) TGA thermogram of extracted collagen (red) and commercial collagen (blue).

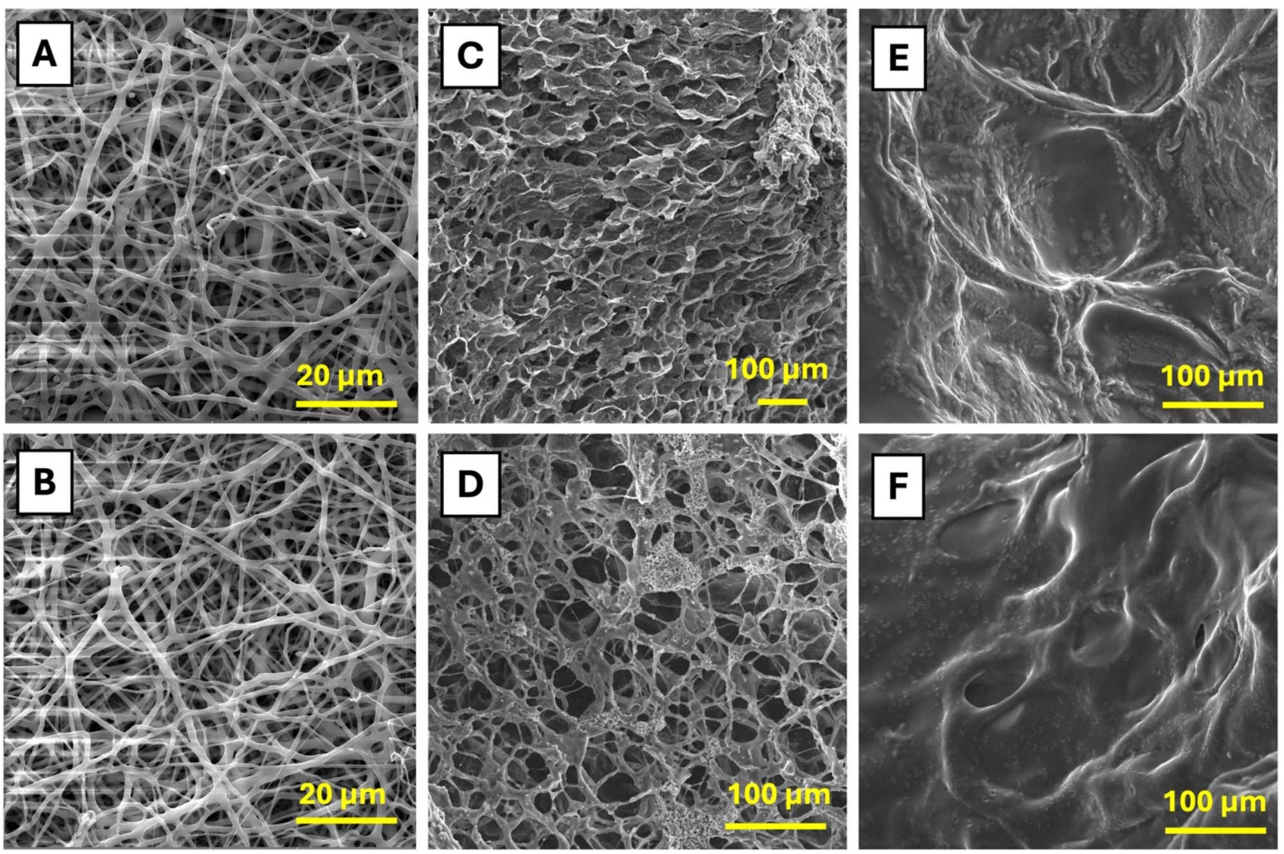


Fig. 4 SEM images of (A) the PDX/PHBV mat and (B) the PDX/PHBV mat supplemented with collagen. SEM images of hydrogel surfaces showing the porous structure of (C) PSucMA and (D) PSucMA with collagen, as well as the surface morphology of (E) the Cel-lig hydrogel and (F) the Cel-lig hydrogel with collagen.

 

An initial mass loss occurred at 50–100 °C (48.4 °C) attributed to a 21% water loss. Collagen denaturation occurred around 200–300 °C with a mass loss of 55% and was in agreement with DSC. The third stage, occurring above 700 °C, corresponded to the protein degradation, resulting in a weight loss of 30%. These observations showed a higher thermal degradation range (200–300 °C) than values reported in the literature, where skin collagen decomposes below 100 °C.[51,61] The TG data of the extracted collagen suggested that extracted collagen was relatively thermoresistant with higher levels of cross-linking and thermostability, thereby displaying better mechanical properties with a degradation temperature between 200 and 750 °C.[60]

**3.1.7 Hydroxyproline analysis.** 4-Hydroxyproline, a neutral heterocyclic protein amino acid, consists of 13.5% of collagen's amino acid composition.[62] The levels of hydroxyproline in fish have been observed to be lower than in mammalian sources.[41,63]

The mechanical properties of collagen as a biomaterial correlate with varying degrees of crosslinking within the protein, especially in the telopeptide region, which influences fibril organization and the protein's tensile strength.[64] The protein's structural integrity, supported by hydroxyproline, content stems from the OH group of its rigid pyrrolidine ring, which initiates hydrogen bonding with other molecules. The hydroxyproline content of the extracted collagen (14.42 ± 0.11%) was higher than that of the soluble commercial collagen (7.91 ± 0.55%), indicating better structural integrity and thermostability.

The results also showed a higher hydroxyproline value than literature values for acid soluble extraction of skipjack tuna with 2.6% from skin,[65] 7.34% from skull[44] and 7.38% from spine.[44]

### 3.2 Engineering and characterization of collagen-loaded scaffolds

Collagen has a hierarchical self-assembled structure with the triple helices aggregated through the formation of fibrils and fibres, stabilized by covalent crosslinks. Upon extraction from natural tissues, the protein is mechanically unstable in aqueous environments as its organization and chemical composition can only partially be reproduced *in vitro*. This mechanical drawback can be countered by appropriate scaffold synthesis to enhance collagen stability *in vitro*.[66]

Six scaffolds were used in this study, namely (i) PDX/PHBV 50/50 nanofiber scaffold, (ii) PSuc-MA hydrogel, (iii) Cel-Lig hydrogel, (iv) PDX/PHBV 50/50 with 10 wt% collagen, (v) PSuc-MA hydrogel with 10 wt% collagen and (vi) Cel-Lig hydrogel with 10 wt% collagen.

**3.2.1 SEM imaging of collagen loaded scaffolds.** The PDX/PHBV 50/50 mat displayed an average fibre diameter of 0.79 ± 0.3 μm and the addition of collagen did not have a major impact on the fibre diameter with an average value of 0.73 ± 0.3 μm (Fig. 4A and B). The addition of collagen to the PSucMA hydrogel enhanced porosity from 334.40 ± 76.18 μm to 408.70 ± 37.28 μm for the collagen loaded PSucMA hydrogel (Fig. 4C and D). The addition of collagen to the Cel-lig hydrogel did not drastically change its surface morphology and topography (Fig. 4E and F). This statement was supported by the evaluation of surface roughness through $R_a$ value calculation. The preliminary image evaluation *via* Fiji/ImageJ revealed that the Cel-lig hydrogel had a surface roughness of 19.51 ± 2.84 and the collagen loaded Cel-lig hydrogel a $R_a$ value of 17.64 ± 3.07 ($p$ > 0.05).

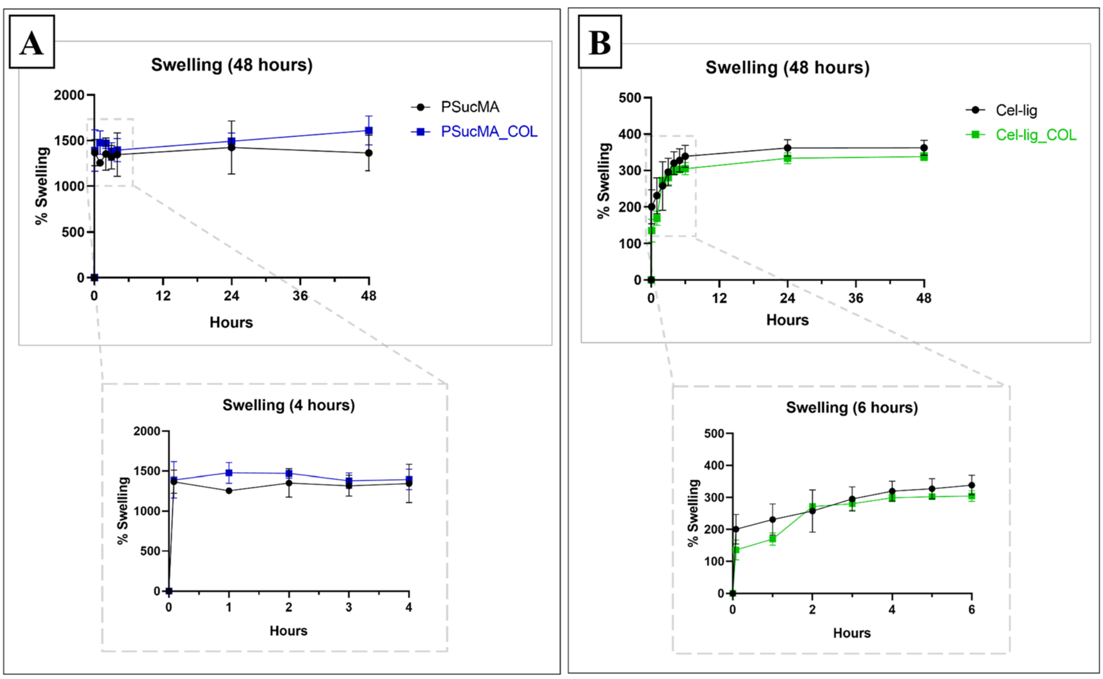


Fig. 5 Percentage swelling of (A) loaded and unloaded PSucMA for 4 hours and 48 hours. (B) Cel-lig hydrogels for 6 hours and 48 hours.

**3.2.2 Surface properties of PDX/PHBV collagen electrospun mats.** The water contact angle of PDX/PHBV 50/50 was found to be 120.0 ± 1.2°. The addition of collagen caused a decrease in the contact angle to 98.2 ± 4.6° and the water drop was absorbed within 20 seconds. Increasing hydrophilicity could provide stable anchor points for the cells and initiate immobilization of protein or growth factors. Cell signalling pathways are triggered following cellular adhesion to the biomaterial. Native collagen as a key component of the ECM facilitates cellular responses through α1β1 and α2β1 integrins and its GFOGER binding motif, which is dependent on the protein's triple helical structure. Integrin subunits such as α5, αV, and α8, which specifically recognize RGD ligands, contribute to cell attachment and signalling.[67,68]

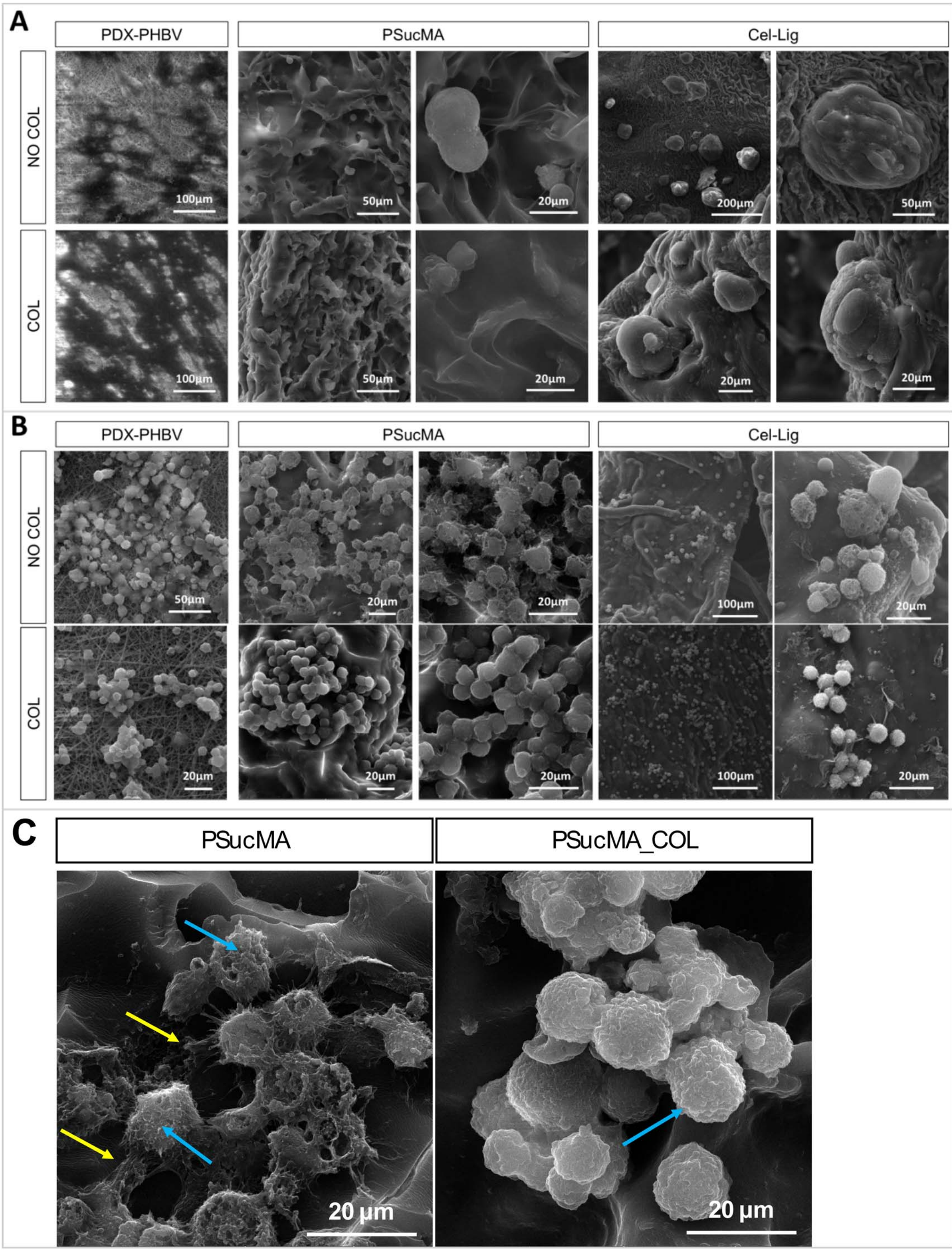


Fig. 6 SEM images showing the morphology of (A) HDF and (B) RAW 264.7 cells on an electrospun PDX/PHBV mat, PSucMA hydrogel and Cel-Lig hydrogels with and without collagen. (C) Mouse macrophage (RAW 264.7) morphologies on PSucMA hydrogels with and without collagen, where yellow arrows demonstrate cytoplasmic extension and blue arrows show cellular ruffling.

 

**3.2.3 Swelling properties of hydrogels.** The swelling properties of the hydrogels provide an indication about their hydrophilic properties and cross-link density. High water content in hydrogels mimics soft natural tissue, which is highly permeable to oxygen and nutrients, resulting in a hydrated environment resembling *in vivo* conditions. Additionally, the mild cooling effect due to the hydrogel's inherent nature can significantly reduce post-operative pain and inflammation. Both loaded and unloaded hydrogels shared similar swelling patterns (Fig. 5). A burst swelling was first observed during the first 30 minutes of submersion in PBS solution, followed by a gradual increase until equilibrium swelling was achieved.

### 3.3 *In vitro* cell studies

The effect of collagen on the adhesion, proliferation and migration of RAW 264.7 macrophages, human dermal fibroblasts (HDFs) and Human Umbilical Vein Endothelial Cells (HUVECs) seeded on the scaffolds was investigated. The proper functioning and metabolism of these cell types are essential at each step of the wound healing pathway, namely in the inflammatory, proliferative and remodelling phases.

**3.3.1 Monoculture of HDFs and RAW 264.7 on scaffolds.** HDF cells attached to and proliferated on all the synthesized scaffolds, irrespective of the presence or the absence of collagen. An increase in the proliferative activity of HDFs in the presence of collagen was clearly observed on the PDX-PHBV electrospun mats (Fig. 6A). It was also observed that HDF cells had the tendency to form spheroids or clusters on the PSucMa and Cel-lig hydrogels with or without collagen.

Cytoplasmic projections and veils surrounding the periphery of macrophages were observed probing the surface of scaffolds without collagen. It was previously demonstrated using SEM images and modelling that these characteristics corresponded to the M1 macrophage phenotype, which indicated activation from M0 to M1.[69] A change in the morphology of mouse macrophages (RAW 264.7) was visible in the presence of collagen for all scaffolds with reduced cytoplasmic projections (Fig. 6C, yellow arrows) and cell ruffling (Fig. 6C blue arrows), corresponding to the M2 or M0 phenotype. M1 phenotype is associated with the pro-inflammatory stage, while M2 is assigned to the anti-inflammatory process in wound healing. These observations might imply that the addition of extracted collagen to the scaffolds could reduce the level of inflammatory response.[27,69] Further investigations have to be conducted to measure the cytokine levels in the culture supernatant and the expression of specific markers using flow cytometry.

**3.3.2 Co-culture of HDFs and HUVECs on scaffolds.** HDFs and HUVECs were stained with fluorescent CellTracker™ green 5-chloromethylfluorescein diacetate (CMFDA) and CellTracker™ red CMTPX, respectively. Both cells were then

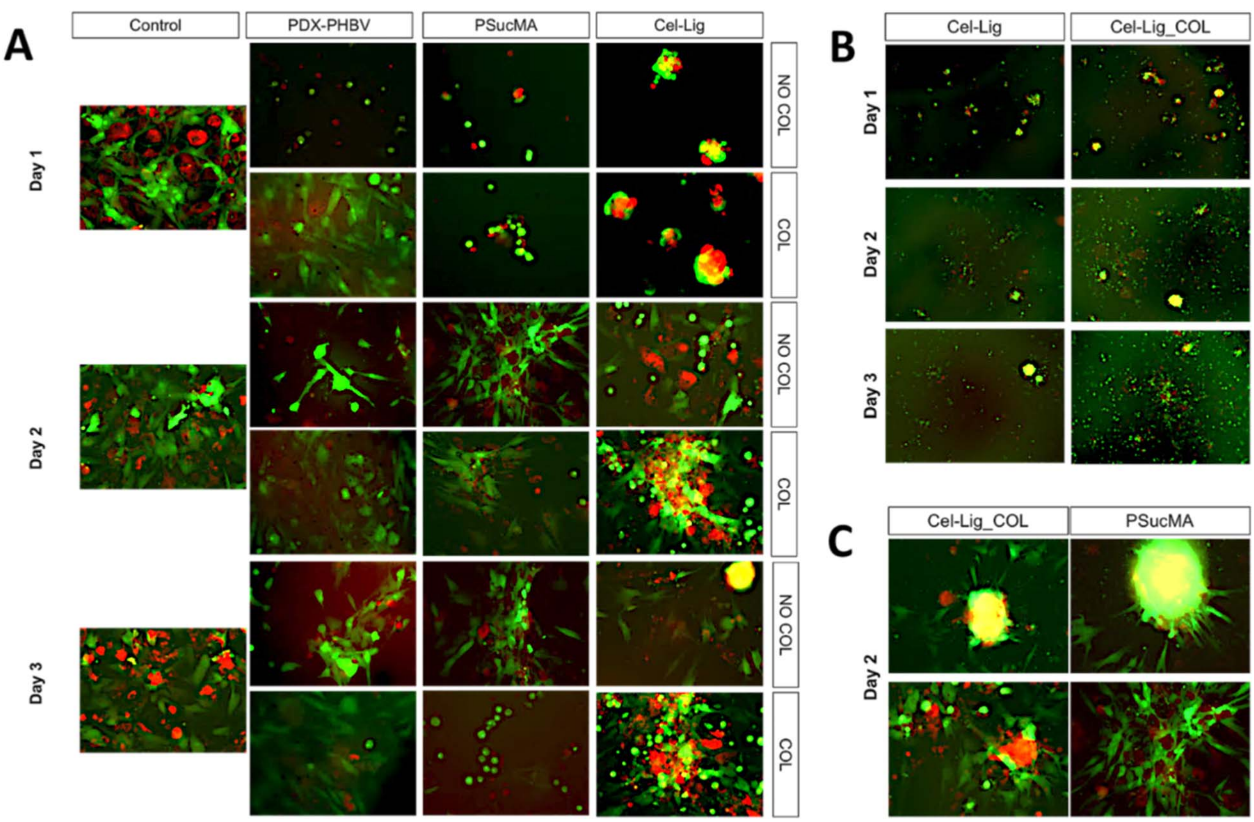


Fig. 7 Fluorescence microscope images of HDFs (green) and HUVECs (red) co-cultured on an electrospun PDX/PHBV mat, PSucMA hydrogel and Cel-Lig hydrogels with and without collagen, where (A) shows images obtained with all tested scaffolds, (B) highlights the presence of cells on the Cel-Lig and Cel-Lig with collagen hydrogels, and (C) presents a zoomed-in view of spheroids on hydrogel samples (Cel-Lig_COL and PSucMA).

seeded on each scaffold at a cell density of $1 \times 10^4$ cells/cell type/scaffold. Fig. 7A shows the fluorescence microscope images of PDX-PHBV mats, PSucMA and Cel-Lig hydrogels seeded with both HDFs and HUVECs on days 1, 2 and 3. HDFs and HUVECs proliferated at a faster rate on PDX-PHBV_COL, with a higher number of cells detected on days 1 and 2 compared to PDX-PHBV mats. A similar observation was noted for the Cel-Lig hydrogel scaffold, where HDFs and HUVECs proliferated to a higher extent on Cel-Lig_COL on days 2 and 3 compared to Cel-Lig hydrogels (Fig. 7B). It is important to note that HUVECs grew better on Cel-Lig hydrogels compared to PDX-PHBV and PSucMA scaffolds. HDFs and HUVECs were seen to interact and grow together within cellular spheroids on both Cel-Lig and PSucMA hydrogels. On days 2 and 3, the cells were scattered and conformed to spindle shapes. These observations suggest that, over time, the cells within the spheroids near the

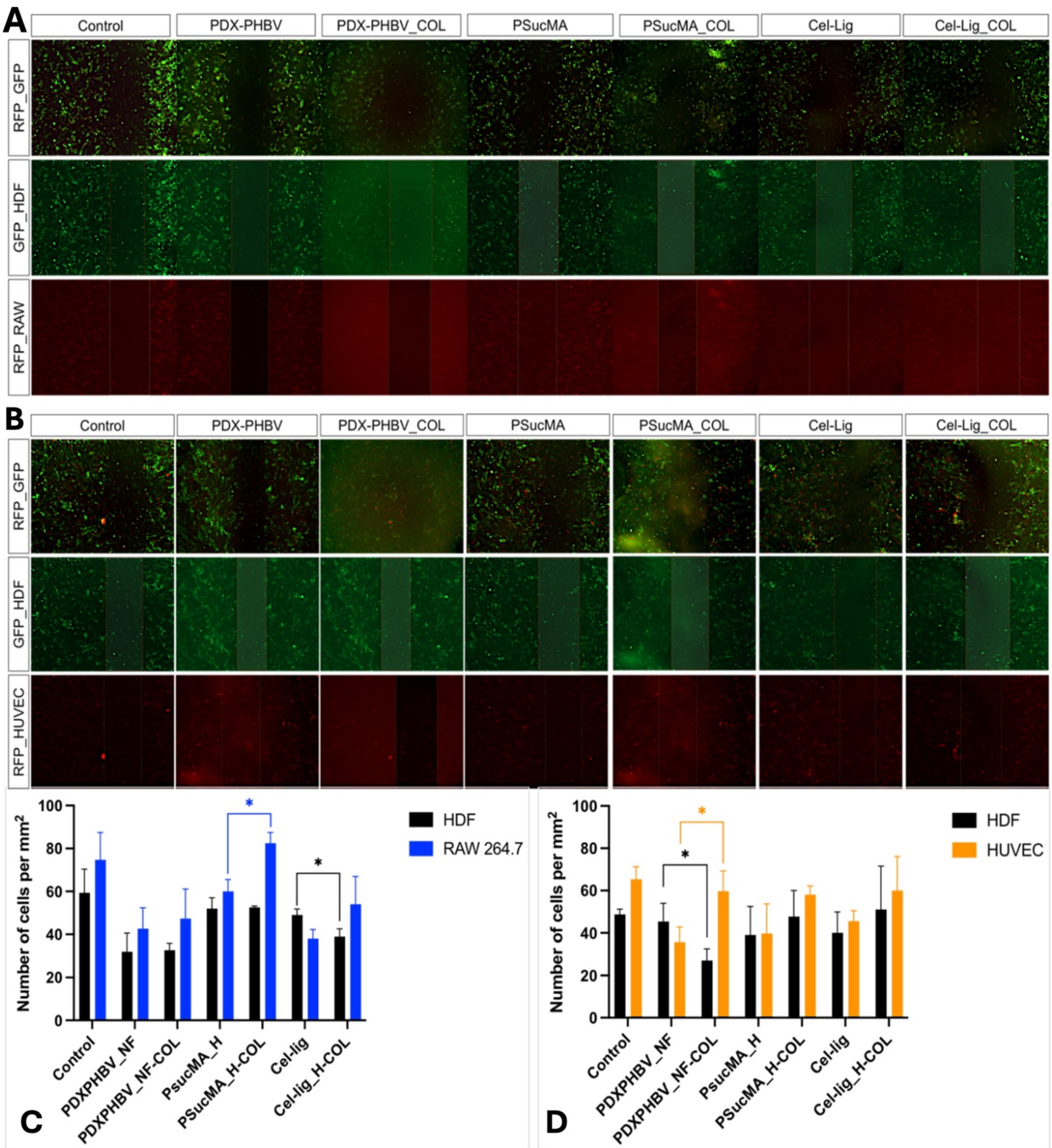


Fig. 8 Fluorescence images of cells migrating within the scratch area: (A) HDF/RAW264.7 and (B) HDF/HUVEC co-cultures. The number of cells per mm$^2$ is graphically represented in (C) for HDFs and RAW 264.7 and in (D) for HDFs and HUVECs, where (*) indicates $p < 0.05$.

 

scaffold interacted with the hydrogel surface, as shown in Fig. 7C. The forces generated by cell–matrix and cell–cell interactions caused the cells to spread and adopt elongated morphologies, making the original spheroid structures no longer visible by day 3. Thus, the cells spread on the scaffolds.

Enhanced growth of HUVECs and HDF cells across all scaffolds loaded with collagen indicated enhanced vascularization, fibroblast proliferation and migration that are needed for events relying on angiogenesis during wound healing.[70]

**3.3.3 *In vitro* scratch assay: HDF co-cultured with RAW 264.7 and HUVECs.** For the *in vitro* scratch assay, a HDF was stained with CellTracker™ Green 5-chloromethylfluorescein diacetate (CMFDA). RAW 264.7 and HUVECs were stained with CellTracker™ Red CMTPX. HDF_RAW264.7 and HDF_HUVECs were co-cultured in 96-well plates at a cell density of $1 \times 10^4$ cells per cell type in each well for 24 h and scratched using a micropipette tip. The sterilized scaffolds were carefully placed in each well and the cells were allowed to proliferate (Fig. 8). The number of cells per mm$^2$ in the scratch region was counted using ImageJ.

Statistical analysis revealed that (i) the presence of collagen in the PSucMA hydrogel enhanced the proliferation and migration of RAW 264.7 cells when cultured with HDFs ($p < 0.05$) and that (ii) collagen within the PDX/PHBV electrospun mat had the tendency to stimulate HUVEC growth in a HDF/HUVEC co-culture system ($p < 0.05$), as illustrated in Fig. 8. Collagen could thus have an impact on (i) vascularization and (ii) stimulation of macrophages that could benefit the production of cytokines for the proper functioning of the wound healing cascade.

## 4 Conclusion

Collagen was successfully extracted from red tuna (skipjack tuna; *Katsuwonus pelamis*) fish skin waste using acetic acid. The extracted collagen consisted of α-tropocollagen chains α1 and α2 (∼120–140 kDa), a β component (∼200 kDa) and a γ component (∼250 kDa). FTIR indicated that the extracted collagen samples displayed amide bands. DSC and TGA analyses showed that extracted collagen exhibited good thermostability and thermoresistant properties. The addition of extracted collagen to three scaffolds (a PDX/PHBV 50/50 mat, PSucMA hydrogel and Cel-lig hydrogel) did not drastically alter their initial physicochemical properties. The potential effect of fluorinated solvents on the collagen structure loaded in the PDX/PHBV 50/50 nanofibers may be further investigated using transmission electron microscopy. Human dermal fibroblast (HDF) cells and human endothelial cells (HUVECs) showed enhanced proliferation on all collagen containing scaffolds. On PSucMA collagen hydrogels, RAW 264.7 showed reduced cytoplasmic extensions and cell ruffling, suggesting a potential decrease in inflammatory response.

## Data availability

Data are available in the paper and ESI.†

## Author contributions

TP – investigation, methodology (extraction and characterization of collagen), formal analysis, visualization, and writing – original draft; MALH – investigation, methodology (*in vitro* experimentation and scaffold fabrication), formal analysis, visualization, and writing – review and editing; DB – investigation, methodology (extraction and advanced characterization of collagen), formal analysis, visualization, and writing – review and editing; ICP and NG – investigation, methodology, and formal analysis; ABL – conceptualization, funding acquisition, methodology development, project administration, and writing – review and editing.

## Conflicts of interest

No conflict of interest was reported by the authors.

## Acknowledgements

The authors would like to thank Ingenia by MCFI (Mauritius) for funding this study and Mrs Patricia D'Unienville, R&D consultant at Ingenia.

## References

1 N. K. Karamanos, A. D. Theocharis, Z. Piperigkou, D. Manou, A. Passi, S. S. Skandalis, D. H. Vynios, V. Orian-Rousseau, S. Ricard-Blum, C. E. H. Schmelzer, L. Duca, M. Durbeej, N. A. Afratis, L. Troeberg, M. Franchi, V. Masola and M. Onisto, *FEBS J.*, 2021, **288**, 6850–6912.
2 H. Zhou, W. Li, L. Pan, T. Zhu, T. Zhou, E. Xiao and Q. Wei, *Regener. Biomater.*, 2024, **11**, rbae008.
3 H. Vilaça-Faria, J. Noro, R. L. Reis and R. P. Pirraco, *Bioact. Mater.*, 2024, **34**, 494–519.
4 N. Meyer, D. V Bax, J. Beck, R. E. Cameron and S. M. Best, *Regener. Biomater.*, 2023, **10**, rbad015.
5 C. Zeltz and D. Gullberg, *J. Cell Sci.*, 2016, **129**, 6.
6 I. Boraschi-Diaz, J. Wang, J. S. Mort and S. V. Komarova, *Front. Phys.*, 2017, **5**, 12.
7 H. Li, J. Tian, H. Cao, Y. Tang, F. Huang and Z. Yang, *Mar. Drugs*, 2023, **21**, 525.
8 F. Jingjing, Y. Qiaolong and L. Xiaoqing, *J. Med. Biochem.*, 2025, **44**, 24–30.
9 Y. Hao, B. Zhao, D. Wu, X. Ge and J. Han, *J. Inflammation Res.*, 2024, **17**, 4993–5004.
10 K. Kukita, N. Matsuzaka, M. Takai, Y. Imamura and Y. Shin, *J. Biochem.*, 2024, **175**, 539–549.
11 Y. Wang, Y. Zhang, T. Li, K. Shen, K. J. Wang, C. Tian and D. Hu, *Adv. Mater.*, 2023, **35**(40), 2303642.
12 E. Sharifi, S. Yousefiasl, N. Laderian, N. Rabiee, P. Makvandi, S. Pourmotabed, M. Ashrafizadeh, F. Familsattarian and W. Fang, *Int. J. Biol. Macromol.*, 2023, **251**, 125898.
13 H. Liu, R. Yang, S. Zhao, F. Zhou, Y. Liu, Z. Zhou, L. Chen and J. Xie, *Bioeng. Transl. Med.*, 2022, **8**(3), e10467.
14 L. Bao, X. Cai, M. Zhang, Y. Xiao, J. Jin, T. Qin and Y. Li, *J. Funct. Foods*, 2022, **90**, 104981.

15 J. Yoon, D. Yoon, H. Lee, J. Lee, S. Jo, D. Kym, H. Yim, J. Hur, W. Chun, G. Kim and Y. S. Cho, *Int. J. Biol. Macromol.*, 2022, **205**, 452–461.
16 S. Benito-Martínez, B. Pérez-Köhler, M. Rodríguez, J. M. Izco, J. I. Recalde and G. Pascual, *Biomedicines*, 2022, **10**, 960.
17 M. M. Murray, L. A. Kalish, B. C. Fleming, B. Flutie, C. Freiberger, R. N. Henderson, G. S. Perrone, L. G. Thurber, B. L. Proffen, K. Ecklund, D. E. Kramer, Y.-M. Yen and L. J. Micheli, *Orthop. J. Sport. Med*, 2019, **7**(3), 2325967118824356.
18 Y.-S. Lim, Y.-J. Ok, S.-Y. Hwang, J.-Y. Kwak and S. Yoon, *Mar. Drugs*, 2019, **17**, 467.
19 A. de Souza, M. de Almeida Cruz, T. A. T. de Araújo, J. R. Parisi, G. C. A. do Vale, K. dos Santos Jorge Sousa, D. A. Ribeiro, R. N. Granito and A. C. M. Renno, *Cell Tissue Res.*, 2022, **388**, 489–502.
20 M. N. Egorikhina, L. L. Semenycheva, V. O. Chasova, I. I. Bronnikova, Y. P. Rubtsova, E. A. Zakharychev and D. Y. Aleynik, *Mar. Drugs*, 2021, **19**, 502.
21 Z. I. Elbialy, A. Atiba, A. Abdelnaby, I. I. Al-Hawary, A. Elsheshtawy, H. A. El-Serehy, M. M. Abdel-Daim, S. E. Fadl and D. H. Assar, *BMC Vet. Res.*, 2020, **16**, 352.
22 J. P. Rodrigues, J. R. da Costa Silva, B. A. Ferreira, L. I. Veloso, L. S. Quirino, R. R. Rosa, M. C. Barbosa, C. M. Rodrigues, P. B. F. Gaspari, M. E. Beletti, L. R. Goulart and N. C. R. Corrêa, *J. Mater. Sci.:Mater. Med.*, 2024, **35**, 12.
23 R. Kaur, A. Jamal, Rishu, H. Kaur, B. Matiyal and R. Kumar, *J. Biol. Act. Prod. from Nat.*, 2023, **13**, 224–237.
24 Y. Ben Azaza, A. van der lee, S. Li, M. Nasri and R. Nasri, *Sustainable Chem. Pharm.*, 2023, **31**, 100905.
25 N. Goonoo, F. Gimié, I. Ait-Arsa, C. Cordonin, J. Andries, D. Jhurry and A. Bhaw-Luximon, *Biomater. Sci.*, 2021, **9**, 5259–5274.
26 I. Chummun, F. Gimié, N. Goonoo, I. A. Arsa, C. Cordonin, D. Jhurry and A. Bhaw-Luximon, *Biomater. Adv.*, 2022, **135**, 112694.
27 M. A. L. Huët, I. C. Phul, N. Goonoo, Z. Li, X. Li and A. Bhaw-Luximon, *J. Mater. Chem. B*, 2024, **12**, 5496–5512.
28 Ł. Kaniuk, K. Berniak, A. Lichawska-Cieślar, J. Jura, J. E. Karbowniczek and U. Stachewicz, *J. Drug Delivery Sci. Technol.*, 2022, **77**, 103855.
29 L. C. Quirino, P. H. de Azambuja Carvalho, R. T. A. Neto, C. A. Comachio, N. G. Monteiro, A. C. Ervolino-Silva, R. Okamoto and V. Pereira-Filho, *Polymers*, 2023, **15**, 868.
30 Ł. Kaniuk and U. Stachewicz, *ACS Biomater. Sci. Eng.*, 2021, **7**, 5339–5362.
31 I. Chummun, D. Bekah, N. Goonoo and A. Bhaw-Luximon, *RSC Med. Chem.*, 2021, **12**, 1476–1490.
32 Y. Jugdawa, A. Bhaw-Luximon, D. Wesner, N. Goonoo, H. Schönherr and D. Jhurry, *React. Funct. Polym.*, 2017, **115**, 18–27.
33 T. L. de Albuquerque, V. G. C. Cavalcante, W. da Silva Rocha, A. C. de Macedo and M. V. P. Rocha, *Int. J. Biol. Macromol.*, 2024, **262**, 130169.
34 D. E. Ciolacu, R. Nicu, D. M. Suflet, D. Rusu, R. N. Darie-Nita, N. Simionescu, G. Cazacu and F. Ciolacu, *Pharmaceutics*, 2023, **15**, 2588.
35 H. Ramphul, A. Bhaw-Luximon and D. Jhurry, *Carbohydr. Polym.*, 2017, **178**, 238–250.
36 I. Chummun Phul, M. A. L. Huët, D. Bekah and A. Bhaw-Luximon, *RSC Med. Chem.*, 2023, **14**, 534–548.
37 D. D. Cissell, J. M. Link, J. C. Hu and K. A. Athanasiou, *Tissue Eng. Part C Methods*, 2017, **23**, 243–250.
38 A. M. E. Matinong, Y. Chisti, K. L. Pickering and R. G. Haverkamp, *Biology (Basel).*, 2022, **11**, 905.
39 J. Wu, L. Kong, J. Zhang and W. Chen, *Pol. J. Environ. Stud.*, 2019, **28**, 2923–2930.
40 S. Indriani, S. Benjakul, H. Kishimura, S. Karnjanapratum and S. Nalinanon, *LWT*, 2022, **162**, 113439.
41 A. R. Leonard, M. H. Cumming, M. A. Ali and J. D. Cabral, *Adv. Funct. Mater.*, 2024, **34**(45), 2405335.
42 W. Firdayanti, W. Trilaksani and S. Purwaningsih, *IOP Conf. Ser. Earth Environ. Sci.*, 2023, **1137**, 012047.
43 S. Chanmangkang, S. Wangtueai, N. Pansawat, P. Tepwong, A. Panya and J. Maneerote, *Polymers*, 2022, **14**, 5329.
44 D. Yu, C.-F. Chi, B. Wang, G.-F. Ding and Z.-R. Li, *Chin. J. Nat. Med.*, 2014, **12**, 712–720.
45 R. O. Sousa, E. Martins, D. N. Carvalho, A. L. Alves, C. Oliveira, A. R. C. Duarte, T. H. Silva and R. L. Reis, *J. Polym. Res.*, 2020, **27**, 73.
46 K. C. R. Carpio, R. S. Bezerra, T. B. Cahú, F. T. D. do Monte, R. C. A. Neri, J. F. da Silva, P. R. dos Santos, R. P. Carvalho, D. M. L. Galeno and A. J. Inhamuns, *Braz. J. Med. Biol. Res.*, 2023, **56**, e12564.
47 Đ. Tintor, K. Ninković, J. Milošević and N. Đ. Polović, *Vib. Spectrosc.*, 2024, **134**, 103726.
48 H. Yang, S. Yang, J. Kong, A. Dong and S. Yu, *Nat. Protoc.*, 2015, **10**, 382–396.
49 M. G. Bridelli, C. Stani and R. Bedotti, *J. Biol. Res. - Boll. della Soc. Ital. di Biol. Sper.*, 2017, **90**(1), 45.
50 T. Tanaka, K. Takahashi, K. Tsubaki, M. Hirata, K. Yamamoto, A. Biswas, T. Moriyama and Y. Kawamura, *Fish. Aquat. Sci.*, 2018, **21**, 7.
51 R. Ahmed, M. Haq and B.-S. Chun, *Int. J. Biol. Macromol.*, 2019, **135**, 668–676.
52 L. A. de Araújo, F. Addor and P. M. B. G. M. Campos, *An. Bras. Dermatol.*, 2016, **91**, 331–335.
53 M. Fernández-Arias, I. Álvarez-Olcina, P. Malvido-Fresnillo, J. A. Vázquez, M. Boutinguiza, R. Comesaña and J. Pou, *Appl. Sci.*, 2021, **11**, 3387.
54 A. Ghofrani and Z. Hassannejad, in*Cell and Molecular Biology*, ed. M. C. Maj and F. Ikolo, IntechOpen, Annual, 2024.
55 E. Badea, T. R. Usacheva and G. Della Gatta, *Russ. J. Chem. Soc.*, 2015, **59**(1–2), 28–41.
56 Y. Zhang, Z. Chen, X. Liu, J. Shi, H. Chen and Y. Gong, *J. Cult. Herit.*, 2021, **48**, 205–210.
57 H. Jafari, A. Lista, M. M. Siekapen, P. Ghaffari-Bohlouli, L. Nie, H. Alimoradi and A. Shavandi, *Polymers*, 2020, **12**, 2230.
58 Y. Dong and Z. Dai, *Mar. Drugs*, 2022, **20**, 550.
59 Q. Zhang, S. Hou, Y. Liu, J. Du, Y. Jia, Q. Yang, T. Xu, Y. Takagi, D. Li and X. Zhang, *Foods*, 2024, **13**, 2901.

 

60 K. V. Srivatsan, N. Duraipandy, R. Lakra, S. K, U. Ramamurthy, P. S. Korrapati and M. S. Kiran, *RSC Adv.*, 2015, **5**, 22106–22116.
61 E. Safitri, O. H. Kuziel, T. Nagai and M. Saito, *Food Chem. Adv.*, 2024, **5**, 100774.
62 A. M. Holwerda and L. J. C. van Loon, *Nutr. Rev.*, 2022, **80**, 1497–1514.
63 H. Ahn, D. J. Gong, H. H. Lee, J. Y. Seo, K.-M. Song, S. J. Eom and S. Y. Yeo, *Polymers*, 2021, **13**, 2151.
64 M. Shayegan, T. Altindal, E. Kiefl and N. R. Forde, *Biophys. J.*, 2016, **111**, 2404–2416.
65 E. Kucukakin, A. C. Adiguzel Zengin, R. Deveci, N. Ork, G. Zengin and B. O. Bitlisli, *Leather Footwear J.*, 2016, **16**, 299–312.
66 G. Tronci, C. A. Grant, N. H. Thomson, S. J. Russell and D. J. Wood, *J. R. Soc. Interface*, 2015, **12**, 20141079.
67 N. Davidenko, C. F. Schuster, D. V. Bax, R. W. Farndale, S. Hamaia, S. M. Best and R. E. Cameron, *J. Mater. Sci.:Mater. Med.*, 2016, **27**, 148.
68 K. M. Pawelec, S. M. Best and R. E. Cameron, *J. Mater. Chem. B*, 2016, **4**, 6484–6496.
69 L. Y. Sujeeun, I. C. Phul, N. Goonoo, N. A. Kotov and A. Bhaw-Luximon, *J. Mater. Chem. B*, 2025, **13**, 3304–3318.
70 R. Costa-Almeida, M. Gomez-Lazaro, C. Ramalho, P. L. Granja, R. Soares and S. G. Guerreiro, *Tissue Eng., Part A*, 2015, **21**, 1055–1065.